Tectonophysics 644–645 (2015) 68–80

Contents lists available at ScienceDirect

Tectonophysics

journal homepage: www.elsevier.com/locate/tecto

Tracking the Oman Ophiolite to the surface — New fission track and (U–Th)/He data from the Aswad and Khor Fakkan Blocks, United Arab Emirates

Joachim Jacobs [a,b,*], Robert J. Thomas [c,1], Anna K. Ksienzyk [a], István Dunkl [d]

[a] University of Bergen, Department of Earth Science, P.O. Box 7803, N-5020 Bergen, Norway
[b] Norwegian Polar Institute, Fram Centre, N-9296 Tromsø, Norway
[c] British Geological Survey, Nicker Hill, Keyworth, Nottingham NG12 5GG, UK
[d] Geoscience Centre, University of Göttingen, Goldschmidtstr. 3, 37077 Göttingen, Germany

ARTICLE INFO

Article history:
Received 30 August 2014
Received in revised form 15 November 2014
Accepted 28 December 2014
Available online 14 January 2015

Keywords:
Oman Ophiolite
Thermochronology
Exhumation
Zagros orogeny
Fission-track analysis

ABSTRACT

The Oman Ophiolite in the United Arab Emirates (UAE) was formed in a supra-subduction zone environment at about 95 Ma and was almost immediately obducted onto the eastern margin of Arabia. The timing of obduction is well constrained, but the post-obduction tectonic, uplift and exhumation history of the ophiolite and associated rocks are less well understood. We present twenty-one new fission track and (U–Th)/He analyses of apatite and zircon from the Hajar Mountains. The data show that the Oman Ophiolite had a complex exhumation history to present exposure levels in the Khor Fakkan and Aswad Blocks, resulting from at least three distinct exhumation events: 1) initial ophiolite obduction between ca. 93 and 83 Ma is characterised by tectonic exhumation and rapid cooling, as revealed by zircon (U–Th)/He and apatite fission-track data, but it is not associated with major erosional exhumation; 2) data from the lower part of the ophiolite and the metamorphic sole document a second exhumation event at ca. 45–35 Ma, interpreted to represent an early phase of the Zagros orogeny that led to reactivation of pre-existing structures and the differential exhumation of the Khor Fakkan Block along the Wadi Ham Shear Zone. This event led to significant erosional exhumation and deposition of a thick sedimentary succession in the Ras Al Khaimah foreland basin; and 3) Neogene exhumation is recorded by ca. 20–15 Ma apatite (U–Th)/He data and a single apatite fission track date from the lowermost part of the metamorphic sole. This event can be linked to the main phase of the Zagros orogeny, which is manifested in large fans with ophiolite-derived debris (Barzaman Formation conglomerates). During this period, the metamorphic sole of the Masafi window stayed at temperatures in excess of ca. 120 °C, corresponding to ca. 4 km of overburden, only later to be eroded to present day levels.

1. Introduction

The Oman Ophiolite complex (aka. the "Semail Ophiolite") is widely acknowledged as Earth's finest example of an obducted ophiolite slab. The Oman Ophiolite formed in a supra-subduction setting and was obducted onto the eastern margin of Arabia in late Cretaceous times (Fig. 1). The complex has been well studied in both Oman and latterly in the United Arab Emirates (UAE) and the geological history up to the time of emplacement on the Arabian continental margin in the UAE is reasonably well known (e.g. Cox et al., 1999; Goodenough et al., 2010, 2014; Nicolas et al., 2000; Peters and Kamber, 1994; Searle and Cox, 1999; Searle et al., 2014; Styles et al., 2006). During obduction high-T metamorphism is recorded in the metamorphic sole footwall rocks with localised melting and the emplacement of small granitic bodies (Styles et al., 2006).

To date however, the post-Cretaceous exhumation and erosion history of the ophiolite is poorly constrained. How much of the ophiolite has been eroded since obduction? What was its initial thickness? How quickly was it eroded to its present level? Were all segments of the ophiolite exhumed at the same time and to the same level? The Khor Fakkan Block shows a slightly deeper lithosphere section (predominated by mantle rocks) than the Aswad Block, from which it is separated by a structural discontinuity. An important question is, when and how the two blocks were finally juxtaposed into their present configuration? The Oman Ophiolite in the UAE lies in a relatively close proximity to the Cenozoic Zagros orogen (Fig. 1), a major mountain belt that resulted from the Palaeogene closure of the Neotethys Ocean and the collision of

* Corresponding author at: University of Bergen, Department of Earth Science, P.O. Box 7803, N-5020 Bergen, Norway. Tel.: +47 45698960.
E-mail address: joachim.jacobs@geo.uib.no (J. Jacobs).
[1] Present address, Council for Geoscience, P.O. Box 572, Bellville 7535, South Africa.

http://dx.doi.org/10.1016/j.tecto.2014.12.018
0040-1951/

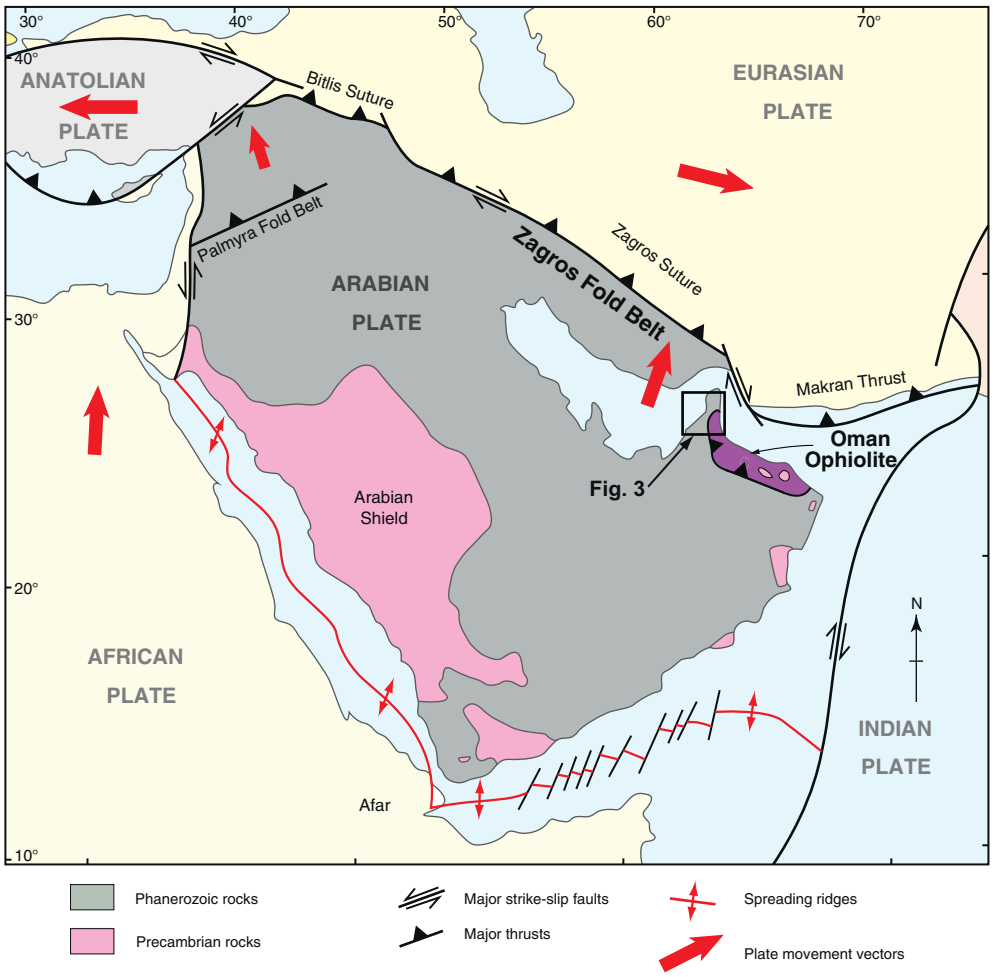

Fig. 1. Architecture of the Arabian Plate: tectonic and geological setting of the Oman Ophiolite, modified from Stern and Johnson (2010).

Arabia with Eurasia. To what extent did the final closure of Neotethys reactivate the ophiolite and did it lead to another exhumation pulse (or pulses) in the various segments? At present, the Oman Ophiolite in the UAE is exposed in the Hajar Mountains, which rise to some 1400 m above sea-level (Fig. 2). It remains unclear precisely when these mountains formed. Are they erosional remnants of the original late Cretaceous obduction phase and/or are they a product of reactivated tectonic uplift and exhumation in the foreland of the Zagros orogeny?

Published low-T thermochronological data, especially fission track and (U–Th)/He analyses of apatite and zircon that could help answer these questions are very sparse in the UAE with only one small dataset available (Tarapoanca et al., 2010). One of the main reasons for this is the shortage of apatite or zircon in the predominantly mafic and ultramafic lithologies. Furthermore, apatite fission track (AFT) analyses are hampered by the low U-contents of apatite in those few rock types where it does occur. This results in a lack of confined track length information for AFT analyses, which in turn prevents viable thermal history modelling. As a result of a major British Geological Survey mapping project between 2002 and 2005 in the UAE Ophiolite (Styles et al., 2006), a vast amount of detailed petrographic information was gained and apatite- and zircon-bearing lithologies and locations were identified. By these means it was possible to obtain enough samples with these minerals to form a representative dataset of AFT, zircon (U–Th)/He (ZHe) and apatite (U–Th)/He (AHe) dates.

2. Geological background

2.1. Geological setting of the Oman Ophiolite

The Oman Ophiolite complex is part of the chain of Alpine ophiolites, which extends across Europe and Asia and preserves remnants of late Palaeozoic to Mesozoic Neotethys ocean crust. It forms a large arcuate outcrop which stretches for over 500 km from the north-eastern coast of Oman, north-westwards to near Dibba in the UAE (Figs. 1 and 3). It has been segmented into 12 individual tectonically-bounded blocks, which include all the main components of a classic ophiolite complex (Lippard et al., 1986). The UAE contains the northernmost two segments, the Khor Fakkan and Aswad Blocks and a small part of the Fizh Block in the south (Fig. 4). The Khor Fakkan and Aswad Blocks are separated by the major Wadi Ham fault zone, which shows several periods of movement, the last of which shows a dextral sense of movement. The Aswad and Fizh Blocks are separated by the Hatta Zone, a faulted-bound sliver of unmetamorphosed Cretaceous continental margin to oceanic volcano-sedimentary rocks, which has been interpreted as having its origins as a transform fault zone (Robertson et al., 1990).

The Oman Ophiolite was obducted generally south-westwards onto the eastern margin of Arabia in late Cretaceous time. The eastern Arabian continental margin comprised Cryogenian crystalline basement unconformably overlain by Ediacaran volcanic and sedimentary rocks, in turn overlain by up to 8 km of Palaeozoic to Mesozoic (Tethyan) rocks

Fig. 2. Typical topography of the Oman Ophiolite in the UAE (Hajar Mountains), reaching up to 1300 m elevation, as seen here, above Zigt village.

(Allen, 2007; Bowring et al., 2007; Thomas et al., 2015). The Phanerozoic rocks include platform carbonates (Musandam Supergroup), which accumulated at a long-lived passive margin. The carbonates pass eastwards into continental slope and deep water Tethyan volcanosedimentary sequences, comprised of the Hamrat Duru Group. These are well exposed in the Dibba and Hatta Zones (Thomas and Ellison, 2014; see Fig. 4). The age of the near shore and offshore sequence can be determined palaeontologically, and the oceanic realm before obduction contained ocean-island carbonatite volcanoes, which have been dated by U–Pb SHRIMP zircon at 103 ± 1 Ma (Grantham et al., 2003).

During and after obduction, the Tethyan slope and oceanic sediments were thrust westwards to south-westwards over the platform carbonates and were highly deformed beneath the advancing ophiolite slab. Obduction caused loading and flexuring of the eastern Arabian margin and the development of two successive foreland basins, filled by late Cretaceous and Cenozoic sediments respectively. In the UAE, the ophiolite is locally underlain by moderate- to high-grade, polydeformed metasedimentary and meta-igneous rocks, which have been interpreted as part of its metamorphic sole (Gnos, 1998; Searle and Malpas, 1982), but might also contain remnants of old continental crustal basement. The metamorphic rocks are well exposed in the Masafi-Ismah window, in an out of sequence thrust slice within the lower part of the ophiolite at Bani Hamid and as a thin tectonic sliver adjacent to the Hatta Zone (Figs. 3, 4). Studies of the northern blocks of the ophiolite (Goodenough et al., 2010, 2014; Lippard et al., 1986; Styles et al., 2006) have documented a complex magmatic history, with the recognition of large volumes of younger, arc-related magmatic rocks ("Phase 2") in addition to the MORB, "Phase 1" ophiolite succession. As a consequence the ophiolite has been modelled as having formed in a "supra-subduction zone" setting.

The Oman Ophiolite in the UAE represents the topmost nappe of the obducted pile. For a general tectonic cross section see Goodenough et al. (2014) and Thomas and Ellision (2014). As the ophiolite arrived at the toe of the continental slope, limestone turbidites of the Hamrat Duru Group were imbricated into a tectonic stack and incorporated into the developing Dibba Zone. The continental margin was telescoped so that an original width of perhaps 250–300 km was shortened to 100 km or less (Thomas and Ellison, 2014). With continuing compression, the ophiolite and the thrust slices of basinal rocks in its footwall, began to impinge on the disrupted edge of the carbonate platform. Continuing westward tectonic transport resulted in a series of fold nappes with a total shortening of around 20–25 km in the Dibba Zone, developing as thrusts propagated through the footwall of the nappe complex. The ophiolite, being rheologically competent and massive relative to the platform, continental slope and deep-sea sediments, is internally relatively undeformed, such that the various magmatic phases and their textures are magnificently preserved in outcrop. In contrast, the rheologically weak metamorphic sole underwent significant ductile deformation at medium- to high-grade metamorphism.

2.2. Timing of ophiolite formation and obduction

The Tethyan MORB oceanic crust of the ophiolite was formed between 97 and 94 Ma, as recorded by U–Pb zircon dates from MORB plagiogranites in Oman (Rioux et al., 2012; Tilton et al., 1981; Warren et al., 2005). In the UAE, the MORB magmatic phase has not been dated, but the age of the Phase 2, supra-subduction magmatism of gabbros and leucotonalite is dated at ca. 96–95 Ma (Goodenough et al., 2010). Thus, MORB magmatism was penecontemporaneous with subduction-related magmatism, supporting a supra-subduction zone model (Goodenough et al., 2014).

The timing of tectonic events, which followed Phase 2 magmatism and led to obduction are less well understood. In the Khor Fakkan Block, the ophiolite lies above medium- to high grade metamorphic rocks that are traditionally regarded as forming the "metamorphic sole", comprising the high grade equivalents of the deep-water volcanosedimentary rocks of the Dibba Zone. A reverse metamorphic gradient is present, with the highest grade rocks at the contact with

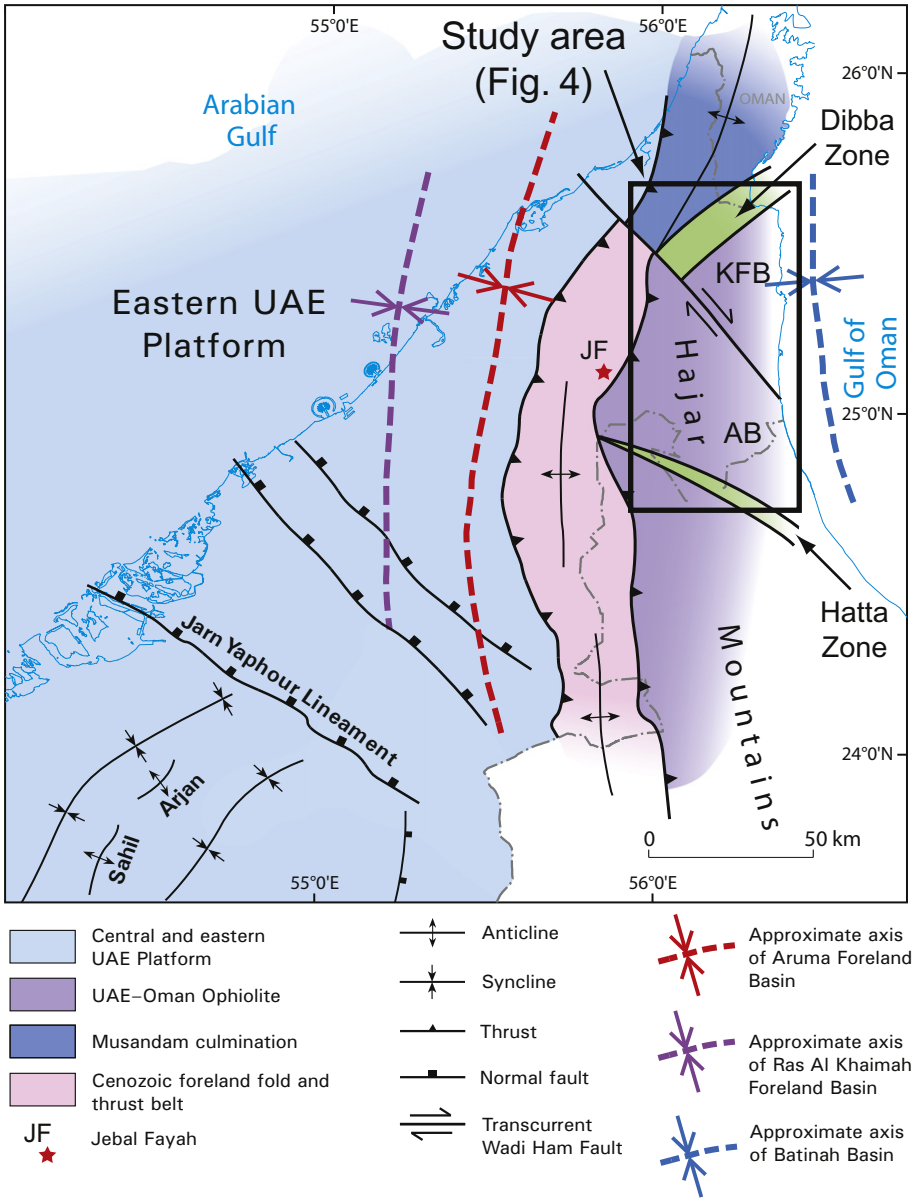

Fig. 3. Location of the study area in the northernmost part of the Oman Ophiolite, showing the main structural domains (modified from Thomas and Ellison, 2014). Abbreviations: AB — Aswad Block, KFB — Khor Fakkan Block.

the base of the ophiolite, decreasing structurally downwards, away from the influence of the overthrust hot mantle nappes (Searle and Malpas, 1982). The metasedimentary rocks at Bani Hamid form a thrust slice within the lower part of the ophiolite that has been metamorphosed to granulite grade with peak P–T conditions of 800–850 °C and 6.5–9 kbar (Gnos and Kurz, 1994), suggesting that the sequence was partially subducted beneath the hot overlying mantle footwall during obduction (Searle et al., 2014). Small melt pods in Bani Hamid amphibolites have been used to date the peak metamorphism at 92.42 ± 0.15 Ma, and small peraluminous granite bodies, intruded into the uppermost mantle harzburgite nappe of the Khor Fakkan Block provided a U–Pb zircon date of 93.22 ± 0.29 Ma (Styles et al., 2006). These dates show that high-grade metamorphism and partial melting due to the early stage of obduction took place very soon after the Phase 2 magmatism. Thus, the entire process of sea-floor spreading, subduction zone magmatism and initiation of obduction onto the eastern continental margin took place within only ca. 2 or 3 Ma. A comparable ultra-high pressure subduction-related event is recorded in Oman much later at about 80 Ma by Warren et al. (2005), showing that subduction–obduction events were not coeval along the length of the ophiolite belt.

Ophiolite obduction in the UAE was initiated at around 93 Ma, but the duration of the process thereafter is only constrained by circumstantial, non-absolute evidence. The westward crustal accretion process loaded the eastern Arabian lithosphere margin and produced a flexural downwarp of the crust (the Aruma foreland basin, Fig. 3), the axis of which migrated westward ahead of the Oman Ophiolite. The Aruma basin was starved of sediment, showing that little clastic detritus was available either from the relatively undisturbed platform in the west or the growing accretionary complex to the east, which did not develop significant orogenic relief at this early stage. As a consequence, the over 2500 m of sediments in the basin (the late Cretaceous Aruma Group) is predominantly limestone mud.

The main phase of deformation associated with the obduction appears to have been completed by the end of the Santonian at about 83 Ma, when Cretaceous orogenesis ceased with the resumption of quiescent limestone sedimentation on the Arabian margin shelf. Immediately

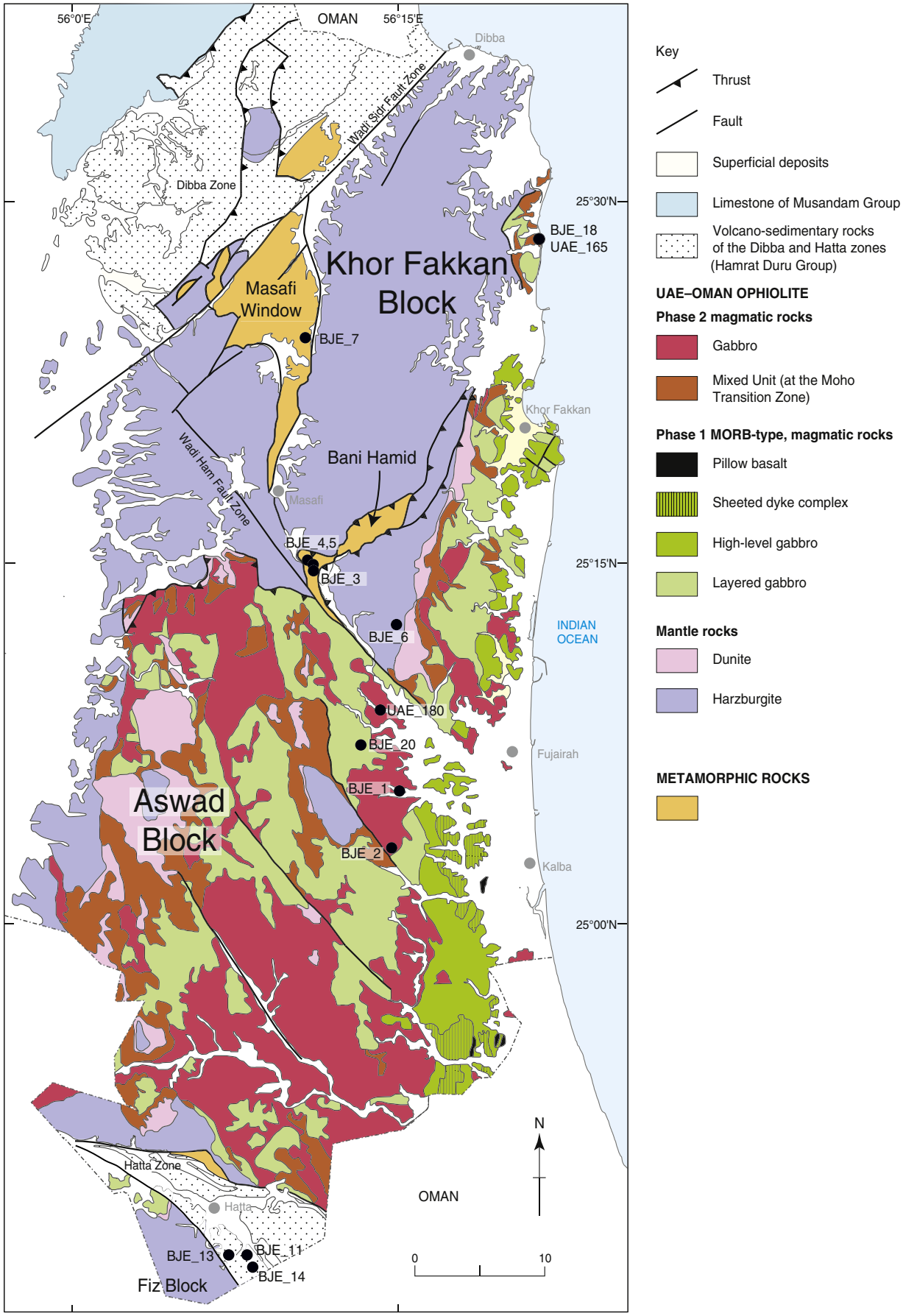

Fig. 4. Geological map of the Khor Fakkan and Aswad Blocks of the UAE Ophiolite, after Goodenough et al. (2010) showing the distribution of the samples from this study.

west of the Hajar Mountains, seismic data show the Aruma Group strata apparently imbricated with the Hamrat Duru Group sediments of the former continental margin, by now part of the westward-propagating nappe stack underlying the ophiolite. A laterite horizon overlying the exposed ophiolite at Jebel Fayah (see Fig. 3) indicates that it must have been uplifted and exposed to sub-aerial weathering during the Campanian or earliest Maastrichtian (ca. 84–72 Ma). The laterite is unconformably overlain by the highest unit of the Aruma Group, the transgressive Simsima Formation of Maastrichtian age (ca. 70 Ma) which oversteps all tectonic units of the Hajar Mountains, from the carbonate platform, across the allochthonous Dibba Zone sequence to rest directly upon the ophiolite.

2.3. Cenozoic final closure of Neotethys and the Zagros orogeny

During the early Cenozoic, Neotethys finally closed, resulting in protracted continental collision between the Afro-Arabian Plate and Eurasia during the Zagros orogeny, which peaked in the Miocene. The Zagros collision is represented in the UAE by two subsiding sedimentary basins; the Ras Al Khaimah foreland basin west of the Hajar Mountains and the extensional Batinah basin east of the mountains (Fig. 3). Two major structural features are associated with the Zagros event; the rising Musandam culmination of the northern Hajar Mountains and a foreland fold and thrust belt, running north-south west of the Hajar Mountains, now mostly covered by Quaternary deposits, but cropping out in anticlinal culminations such as those of Jebels Hafit and Fayah. The late Cretaceous structures such as the thrusts associated with ophiolite obduction, the nappes of the Dibba Zone foreland fold and thrust belt and the transpressive Hatta Zone were probably rejuvenated at this time.

The Ras Al Khaimah Basin trended north–south in the mountain front region near Sharjah and Dubai and extended into the Arabian Gulf and into the Fars Province of south-eastern Iran. The basin developed as a response to renewed loading of the NE margin of the Arabian plate in a similar fashion to that which initiated the Aruma basin in late Cretaceous times as a result of the early stages of the closure of Neotethys. The basin is filled with up to 2000 m of the Palaeocene to late Eocene sediments (Hasa Group). The eastern margin of the Ras Al Khaimah Basin was probably controlled by west-verging, syn-depositional faults and thrusts at the edge of the mountain front, coupled with the uplift of the Musandam flexure and illustrated by the occurrence of large allochthonous blocks of ophiolite and syn-sedimentary conglomerate within the Palaeocene (ca. 66 to 56 Ma) Muthaymima Formation, turbidites within the Pabdeh Group and syn-depositional slumps within the Rus Formation. Later in the Eocene and Oligocene, subsidence of the Ras Al Khaimah Basin seems to have slowed and the Dammam and Asmari Formations reflect re-establishment of the shallow-marine carbonate shelf between ca. 25 and 23 Ma.

The Neogene foreland fold and thrust belt, which developed mainly on the eastern limb of the Ras Al Khaimah Basin, west of the Hajar Mountains, are almost entirely covered by Quaternary deposits, although its distribution and many of its structures are well shown by geophysical surveys (e.g. Farrant et al., 2012). It forms an arcuate belt approximately 30 km wide, which runs from the Gulf coast north of Ras Al Khaimah for about 200 km southwards to the Al Ain area and southwards into Oman. The structures are characterised by west-verging geophysical discontinuities interpreted as thrusts and very tight folds with wavelengths up to about 3 km, exposed in a number of north–south trending *en-echelon*, periclinal domes deforming strata as young as Miocene (Barzaman Formation: ca. 15–12 Ma) in age.

2.4. Previous thermochronology Oman Ophiolite, UAE

An extensive Ar–Ar thermochronological study and a review of previous K–Ar and Ar–Ar work on hornblende, muscovite, biotite and K-feldspar across large parts of the ophiolite have been provided by Hacker et al. (1996). North of 24.5° N (in the UAE), 18 K–Ar and Ar–Ar dates on a range of minerals are available from this study. Five hornblende samples gave plateau ages ranging from 99–92 Ma. North of the Hatta Zone, three muscovite plateau ages range from 91–90 Ma, whilst typical muscovite plateau ages south of the Hatta Zone are slightly older at 93–94 Ma. Biotite separates did not provide plateau ages and their total fusion ages scatter significantly from 128–63 Ma, with three ages at the lower age range between 80 and 63 Ma. One K-feldspar plateau age of 63 Ma is available south of the Hatta Zone. The hornblende and muscovite ages are interpreted to reflect rapid cooling of the ophiolite to temperatures below ca. 350 °C, whilst the biotite and K-feldspar ages, despite their large scatter might indicate a low-T overprint, probably related to post-emplacement folding. The ophiolite underwent folding and cleavage development in latest Maastrichtian to early Palaeocene times (68–64 Ma) (Rabu, 1993, in Hacker et al., 1996), after which a period of quiescence started.

Only one previous fission track study of the UAE segment of the Oman Ophiolite has been published. Tarapoanca et al. (2010) reported one zircon and four apatite fission-track ages. AFT ages range from ca. 75 Ma–20 Ma. From one sample, both a zircon and an apatite fission-track age of ca. 45 Ma are reported, suggesting rapid cooling at that time. No track length information was reported from this study, so no thermal history modelling could be provided. An unpublished AHe age of ca. 20 Ma is reported from the Bani Hamid metamorphic sole (Gray et al., 2006) and 6 AFT ages of ca. 45–35 Ma with very limited track-length information are presented in an unpublished report (Grantham et al., 2003).

3. Samples and analytical methods

Apatite and zircon-bearing lithologies include tonalitic rocks and "vinaigrettes" (igneous breccias related to the second phase of magmatism in the ophiolite), S-type granites associated with the obduction event, carbonatites intruded into oceanic volcano-sedimentary rocks connected with the ophiolite, various metamorphic sole units of the Bani Hamid Group (quartzites, quartz schists, amphibolites) and the Masafi Schists. Altogether 20 samples were collected from the Khor Fakkan and Aswad Blocks. Field photographs of typical sampled lithologies are given in Fig. 5.

Apatite and zircon were separated using standard mineral separation techniques, including a Wilfley table, magnetic and heavy liquid separation. Fifteen samples yielded enough apatite or zircon of sufficiently good quality for AFT, ZHe and AHe dating. Apatite grains from 11 samples were analysed by the AFT method. Five of these also provided AHe analyses and another five samples gave ZHe data.

3.1. AFT analysis

AFT analyses were performed at the Department of Earth Science, University of Bergen, Norway. Grains were embedded in epoxy blocks, which were ground and polished to expose internal crystal surfaces. The samples were etched in 5 M nitric acid for 20 s at 20 ± 0.5 °C. Uranium contents were determined using the external detector method as described by Gleadow (1981). Irradiation was conducted at the FRM II research reactor at the Technical University of Munich, using a thermal neutron flux of 10^{16} neutrons/cm^2. Dosimeter glasses IRMM-540R (15 ppm U) were used to monitor the neutron flux. Induced tracks in the micas were revealed by etching in 40% hydrofluoric acid for 20 min at room temperature. To increase the number of etchable confined tracks, an aliquot of four samples (two from each of the main blocks) were irradiated with ^{252}Cf at the School of Earth Sciences, University of Melbourne, Australia.

To determine AFT ages, the zeta calibration approach was applied (Hurford and Green, 1983). A personal zeta factor of 233.56 ± 3.27 was established by counting Durango and Fish Canyon Tuff standards. Spontaneous and induced fission tracks were counted using an Olympus BX51 optical microscope at a total magnification of 1250×. The microscope was equipped with a computer-controlled stage, utilizing the FT-Stage software (Dumitru, 1993). AFT ages were calculated with TrackKey (Dunkl, 2002). Confined track lengths were measured at a magnification of 2000× and corrected by c-axis projection (Ketcham et al., 2007a). Only

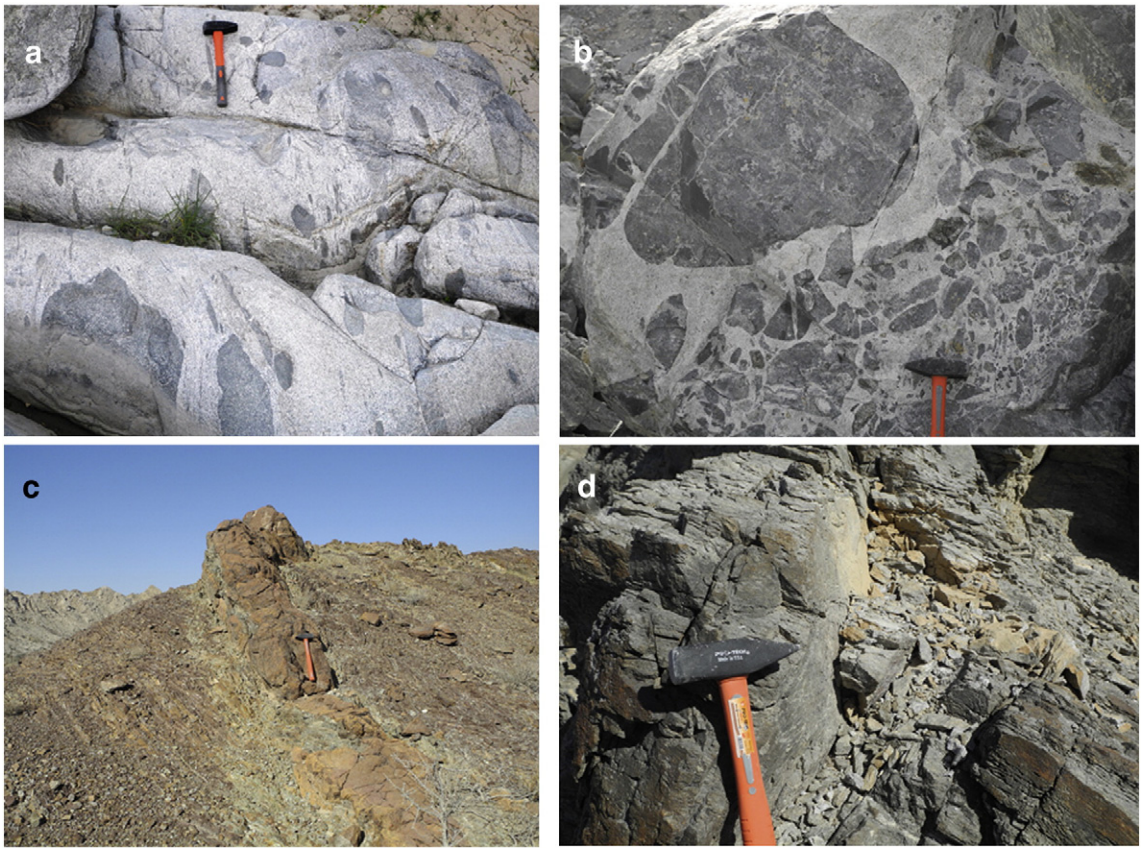

Fig. 5. Field photographs of typical analysed lithologies. a) Tonalite of Phase 2 magmatism; b) leucotonalite–dolerite magmatic breccia "vinaigrette"; c) carbonatite dyke intruded into deep sea cherts of the Hatta Zone; and d) impure quartzite in the Bani Hamid metamorphic slice.

horizontal TINT-type tracks (Lal et al., 1969) in apatite grains that were oriented parallel to the crystallographic c-axis were measured. Etch pit diameters (Dpar; Donelick et al., 2005) were also measured at 2000× and were used as a proxy for apatite chemistry and thus annealing behaviour.

3.2. ZHe and AHe analysis

ZHe and AHe analyses were conducted at the Geoscience Centre, University of Göttingen, Germany. Three to five single crystals were hand-picked from each sample using binocular and petrographic microscopes. The selected crystals all show well-defined external morphologies and are (as much as possible) free of inclusions. The length and width of each crystal were measured, and the grains were then packed in individual platinum capsules. He-degassing was performed under high vacuum by heating with an infrared diode laser. After purification with a SAES Ti–Zr getter at 450 °C, the extracted gas was analysed with a Hiden triple-filter quadrupole mass spectrometer, equipped with a positive ion counting detector. To ascertain a quantitative helium extraction, a re-extraction was performed for every sample.

To analyse the ^{238}U, ^{232}Th and Sm contents, the platinum capsules were retrieved after He analysis. Zircons were dissolved in pressurized Teflon bombs using a mix of 48% HF + 65% HNO_3 for 5 days at 220 °C. Apatite crystals were dissolved in 2% HNO_3 at room temperature in an ultrasonic bath. The dissolved crystals were spiked with calibrated ^{230}Th and ^{233}U solutions and analysed by the isotope dilution method on a Perkin Elmer Elan DRC ICP-MS equipped with an APEX micro flow nebuliser. Form-dependent alpha-ejection corrections (F_T correction) were applied to all raw (U–Th)/He ages, following the procedures of Farley et al. (1996) and Hourigan et al. (2005).

3.3. Thermal history modelling

Thermal history modelling was performed with HeFTy 1.8.3 (Ketcham, 2005). For modelling of the apatite age and confined track length data, the annealing model of Ketcham et al. (2007b) was used. C-axis parallel etch pit diameters (Dpar) were used as the kinetic parameter (Donelick et al., 2005). For modelling of AHe data, the calibration of Farley (2000) was used. AFT and AHe data were modelled together. For the AHe data, we used mean values of the single grain analyses, including mean ages, grain radii and U, Th and Sm concentrations. In the study area there are very few independent constraints of the thermal evolution available. For the main body of the ophiolite, consistent ZHe ages of ca. 75 Ma (see below) were used as modelling constraints at the higher temperature end. For each sample 500,000 random paths were run. The quality of the modelling results is expressed as goodness of fit for AFT ages, confined track lengths and AHe ages (Fig. 7).

4. Results

4.1. AFT ages

The AFT ages obtained range from late Cretaceous to early Oligocene (87–31 Ma) and show no correlation between either age and U-concentration or age and the kinetic parameter of track annealing (Dpar) (Table 1). Most of the samples have relatively low U-concentrations and therefore also low track densities. This results in low track counts (poor counting statistics) and consequently relatively widely spread single grain ages and large single grain age uncertainties. All samples passed the χ^2-test, indicating that statistically only one age population is present in each sample. However, in some samples this might be attributed to the large single grain age

Table 1
Apatite fission track data.

Sample no.	Lithology	Easting	Northing	Elev. (m)	N (G)	Spontaneous ρ_s	Spontaneous N_s	Induced ρ_i	Induced N_i	Dosimeter ρ_d	Dosimeter N_d	P(X^2) (%)	Disp.	U (ppm)	Dpar (μm)	Age[a] (Ma)	±1σ (Ma)	Measured MTL (μm)	Measured ±1σ (μm)	N (TL)
BJE-01	Tonalite	425913	2776154	155	24	4.68	195	12.45	519	19.87	32,890	54	0.04	14	1.27	**87**	**7**			
BJE-02	Tonalite	424733	2771325	290	18	4.60	123	12.61	337	19.83	32,890	57	0.00	15	1.46	**84**	**9**			
BJE-03	Bani Hamid P4 quartzite	418482	2793274	530	5	2.20	20	8.14	74	19.79	32,890	60	0.03	5	1.33	**62**	**16**			
BJE-04	Bani Hamid P4 quartz schist	418857	2793243	465	9	2.34	64	15.30	418	19.75	32,890	52	0.00	13	1.23	**35**	**5**			
BJE-05	Bani Hamid P4 quartzite	419099	2792826	365	25	6.20	319	41.89	2154	19.70	32,890	97	0.00	31	1.32	**34**	**2**	12.16	1.93	84
BJE-06	Granite	425436	2788906	320	26	3.68	196	24.25	1292	19.66	32,890	65	0.00	18	1.21	**35**	**3**	12.59	1.49	83
BJE-07	Carbonatite	418019	2811383	345	26	2.92	211	21.81	1578	19.62	32,890	76	0.03	16	2.72	**31**	**2**			
BJE-11	Carbonatite	415818	2740030	355	30	1.72	226	6.34	832	19.57	32,890	73	0.10	8	3.26	**63**	**5**			
BJE-13	Carbonatite	413853	2741200	245	30	1.42	142	6.28	627	19.53	32,890	24	0.27	5	3.31	**58**	**7**	13.72	1.31	80
BJE-14	Carbonatite	415537	2740625	365	24	1.50	138	8.48	783	19.49	32,890	97	0.00	12	3.09	**40**	**4**	13.80	1.58	77
BJE-20	Felsic vinaigrette	423196	2779380	235	7	7.50	62	22.74	188	19.43	32,890	46	0.08	16	2.50	**74**	**11**			

MTL — mean track length; N (G) — number of dated grains; N (TL) — number of measured track lengths; Ns, i, d — number of tracks counted; ρs, i, d — track densities in 1×10 tracks/cm^2.
[a] Central age.

uncertainties, as is discussed below. Since all samples were collected below 550 m altitude, an elevation effect can be disregarded.

The oldest ages of 87–74 Ma were obtained from three tonalite samples (BJE_01, 02, 20) from the north-eastern part of the Aswad Block, upper part of the ophiolite. These samples display relatively wide unimodal single grain age distributions. The ages are thought to represent cooling following ophiolite obduction. However, no track length information is available for these samples to provide additional information on the nature of this cooling event.

The youngest AFT ages come from various lithological units from the lower part of the ophiolite and from the metamorphic sole (Bani Hamid Group metamorphic rocks, Masafi Schist, S-type granite and carbonatite), exposed in the Khor Fakkan Block. Four samples gave late Eocene to early Oligocene ages between 35 and 31 Ma (BJE_04, 05, 06, 07). These samples display narrow unimodal single grain age distributions. Mean track lengths for samples BJE_05 and 06 are 12.2 μm and 12.6 μm respectively. Since these ages are much younger than those found in the upper part of the ophiolite, these samples probably underwent resetting at the base of the ophiolite, followed by cooling during the Eocene. The shortened track lengths indicate that the samples spent some time in the partial annealing zone and the onset of cooling most likely pre-dates the actual AFT ages. A fifth sample (BJE_03) gave an older age of 62 Ma. However, apatite crystals from this sample were of poor quality and only five grains could be dated. The reliability of this age may therefore be questionable.

The remaining three samples (carbonatites BJE_11, 13, 14) were collected from the Hatta Zone south of the Aswad Block. These samples yielded ages between 64 and 40 Ma. Samples BJE_13 and 14 gave longer mean track lengths than the samples from the Khor Fakkan Block of 13.7 μm and 13.8 μm respectively. The apatite in these carbonatites has an unusual chemistry, which is reflected in very large etch pit diameters (>3 μm). U-concentrations in these samples are low (on average 5–12 ppm, but most grains <3 ppm), resulting in a wide spread of single grain ages and large single grain age uncertainties. The samples show strongly skewed to bimodal single grain age distributions. However, this effect is obscured by the large single grain age uncertainties and the samples pass the χ^2-test. The significance of a possible bimodality in the single grain apatite ages is therefore uncertain.

4.2. ZHe ages

ZHe analyses of five samples (3–4 grains per sample) from both the Khor Fakkan and Aswad Block mostly yielded late Cretaceous ages (Table 2). Sample BJE_01 gave three single grain ages between 75 and 66 Ma with a mean age of 72 Ma. Sample BJE_18 yielded two single grain ages of 84 and 79 Ma respectively and a much older single grain age of 172 Ma. The latter is excluded as an outlier and a mean age of 81 Ma is used for the sample. Three single zircons from sample BJE_20 gave ages between 75 and 81 Ma with a mean age of 79 Ma. A fourth grain from this sample gave a younger age of 47 Ma but was excluded as an outlier. Sample UAE_165 produced three single grain ages between 69 and 85 Ma and a mean age of 77 Ma, and finally sample UAE_180 yielded three single grain ages between 65 and 77 Ma with a mean age of 71 Ma. Mean sample ages thus range from 71–81 Ma and show no significant difference between the Khor Fakkan and Aswad Blocks. These ages are essentially coeval with the oldest AFT ages, probably indicating rapid cooling in late Cretaceous times.

4.3. AHe ages

Five samples were AHe dated, with 4–5 grains per sample (Table 2). One sample comes from the upper part of the ophiolite (BJE_02), two samples come from the lower part of the ophiolite and metamorphic sole respectively (BJE_06, 05), and the final two samples come from the Hatta Zone (BJE_13, 14). Out of a total of 22 single grain analyses, two were excluded because the U- and Th-concentrations were below the detection limit. The majority of the remaining 20 apatites provided Oligocene to mid-Miocene ages.

Sample BJE_02 gave three single grain ages between 14 and 16 Ma, with a mean age of 15 Ma. Sample BJE_05 yielded three single grain ages between 15 and 24 Ma and a mean age of 19 Ma. The five apatite grains of sample BJE_06 fall into two groups: the three younger grains provide single grain ages between 14 and 25 Ma and a mean age of 19 Ma, whilst the remaining two analyses are significantly older (54 and 77 Ma). The ages are not correlated with either grain size or effective U-concentration. However, the quality of the apatite in this sample

Table 2
Apatite and zircon (U–Th)/He data.

			He		U			Th				Sm			Ejection	*Uncorr.*	Ft-Corr.		Sphere	Unweighted sample average [Ma]	
Sample	Lithology Easting	Northing	Vol. [ncc]	1σ [%]	Mass [ng]	1σ [%]	Conc. [ppm]	Mass [ng]	1σ [%]	Conc. [ppm]	Th/U ratio	Mass [ng]	1σ [%]	Conc. [ppm]	correct. (Ft)	*He-age [Ma]*	He-age [Ma]	1σ [Ma]	radius [μm]	Age	±1 s.e.
BJE-02 a1	Tonalite		0.020	5.2	0.013	4.7	13.4	0.007	3.7	7.5	0.56	0.524	5.9	531	0.56	*8.7*	**15.5**	**1.4**	36		
BJE-02 a2	424733	2771325	0.013	6.2	0.007	9.0	7.7	0.004	4.1	4.4	0.58	0.314	6.2	350	0.72	*10.4*	**14.4**	**1.4**	52		
BJE-02 a3			0.027	4.3	0.022	3.3	23.4	0.013	3.3	13.5	0.58	0.455	6.0	490	0.58	*8.0*	**13.8**	**1.1**	37	14.5	0.5
BJE-05 a1	Bani Hamid P4		0.021	4.5	0.009	6.4	3.1	0.004	5.1	1.3	0.43	0.763	4.2	250	0.68	*10.4*	**15.3**	**1.2**	50		
BJE-05 a2	419099	2792826	0.274	1.7	0.120	1.9	30.0	0.003	5.5	0.7	0.02	0.837	3.9	210	0.74	*17.8*	**24.1**	**1.1**	60		
BJE-05 a4			0.009	6.0	0.004	17.0	4.7	0.003	5.8	2.9	0.62	0.197	4.9	211	0.57	*11.1*	**19.5**	**2.7**	37	19.6	2.6
BJE-06 a1	Granite		0.085	2.4	0.009	7.5	8.9	0.025	2.8	25.1	2.81	0.216	6.1	220	0.55	*42.7*	77.4	6.3	36		
BJE-06 a2	425436	2788906	0.103	2.3	0.024	2.9	18.9	0.004	5.3	3.0	0.16	0.245	5.3	194	0.59	*31.7*	53.7	3.8	38		
BJE-06 a3			0.012	5.6	0.009	6.8	11.2	0.006	4.1	8.0	0.71	0.173	5.5	215	0.50	*8.6*	**17.2**	**1.8**	31		
BJE-06 a4			0.037	3.8	0.018	3.7	27.8	0.003	4.2	5.37	0.19	0.204	3.5	314	0.59	*14.8*	**25.1**	**2.0**	38		
BJE-06 a5			0.004	10.1	0.002	38.9	1.6	0.006	4.0	4.73	2.91	0.155	4.2	131	0.61	*8.3*	**13.5**	**2.7**	42	18.6	3.4
BJE-13 a1	Carbonatite		0.177	1.9	0.011	5.6	2.3	0.128	2.5	27.0	11.57	0.711	4.2	150	0.80	*31.0*	38.7	1.6	78		
BJE-13 a2	413853	2741200	0.071	2.6	0.005	13.6	2.1	0.056	2.5	24.1	11.43	0.348	4.7	149	0.79	*27.9*	35.4	1.9	73		
BJE-13 a3			0.082	2.4	0.013	4.7	2.3	0.143	2.5	24.7	10.92	0.850	4.0	147	0.84	*12.6*	**15.1**	**0.6**	96		
BJE-13 a4			0.052	2.7	0.010	6.4	2.3	0.095	2.5	22.7	10.02	0.576	4.5	137	0.84	*11.7*	**13.9**	**0.6**	99		
BJE-13 a5			0.060	3.2	0.007	8.6	2.5	0.089	2.5	31.47	12.55	0.518	2.7	184	0.81	*15.3*	**18.9**	**0.9**	84	16.0	1.5
BJE-14 a1	Carbonatite		0.024	3.9	0.006	11.7	2.1	0.035	2.6	12.0	5.71	0.422	5.1	143	0.79	*11.2*	**14.1**	**0.9**	75		
BJE-14 a2	415537	2740625	0.061	2.7	0.011	5.6	3.1	0.077	2.5	21.3	6.98	0.638	4.3	177	0.82	*14.7*	**18.0**	**0.8**	88		
BJE-14 a3			0.078	2.6	0.014	4.6	2.2	0.088	2.5	14.4	6.54	0.885	4.3	144	0.82	*15.4*	**18.8**	**0.8**	88		
BJE-14 a4			0.069	2.4	0.014	4.5	3.6	0.085	2.5	21.9	6.14	0.707	4.4	181	0.80	*14.3*	**17.9**	**0.8**	78	17.2	1.1
BJE-01 z1	Tonalite		5.27	0.9	0.862	1.8	262	0.153	2.4	47	0.18	0.006	27.1	2	0.74	*48.4*	**65.7**	**2.9**	46		
BJE-01 z2	425913	2776154	2.80	1.0	0.383	1.8	85	0.061	2.5	13	0.16	0.004	38.1	1	0.77	*58.0*	**75.4**	**3.0**	53		
BJE-01 z3			2.88	1.0	0.409	1.8	107	0.079	2.4	21	0.19	0.004	38.0	1	0.75	*55.5*	**73.8**	**3.1**	49	71.6	3.0
BJE-18 z1	Granite		22.31	0.9	1.210	1.8	544	1.281	2.4	576	1.06	0.072	8.5	32	0.70	*120.9*	172.1	8.2	41		
BJE-18 z2	435720	2817410	21.80	0.9	2.588	1.8	1377	2.190	2.4	1165	0.85	0.026	11.1	14	0.69	*57.9*	**84.0**	**4.2**	39		
BJE-18 z3			23.45	0.9	2.958	1.8	1314	2.356	2.4	1047	0.80	0.053	9.8	23	0.70	*55.0*	**78.8**	**3.8**	40	81.4	3.7
BJE-20 z1	Felsic vinaigrette		13.40	1.1	1.798	1.8	303	0.512	2.4	86	0.28	0.074	8.8	12	0.76	*57.5*	**75.4**	**3.1**	52		
BJE-20 z2	423196	2779380	5.71	1.1	0.756	1.8	172	0.120	2.4	27	0.16	0.009	22.4	2	0.75	*60.0*	**79.9**	**3.4**	49		
BJE-20 z3			0.64	1.3	0.146	2.1	51	0.028	2.7	10	0.19	0.002	78.3	1	0.74	*34.9*	47.3	2.2	46		
BJE-20 z4			2.37	1.0	0.333	1.9	126	0.028	2.7	11	0.08	0.001	70.1	0	0.71	*57.5*	**80.9**	**3.9**	42	78.7	1.7
UAE165 z1	Granite		16.10	1.1	2.279	1.8	886	1.194	2.4	464	0.52	0.027	14.0	10	0.69	*51.9*	**75.7**	**3.9**	38		
UAE165 z2	435720	2817410	18.65	1.1	2.179	1.8	476	1.244	2.4	272	0.57	0.029	13.6	6	0.74	*62.2*	**84.5**	**3.7**	46		
UAE165 z3			11.04	1.1	1.721	1.8	818	0.735	2.4	349	0.43	0.019	13.5	9	0.69	*48.1*	**69.3**	**3.5**	39	76.5	4.4
UAE180 z1	Felsic vinaigrette		2.72	1.2	0.372	1.9	114	0.081	2.4	25	0.22	0.013	16.2	4	0.74	*57.2*	**77.4**	**3.4**	46		
UAE180 z2	423702	2781090	0.85	1.4	0.153	2.1	123	0.025	2.6	20	0.17	0.010	19.8	8	0.64	*44.1*	**69.3**	**4.1**	32		
UAE180 z3			1.64	1.3	0.276	1.9	79	0.051	2.5	15	0.18	0.005	22.1	1	0.73	*47.1*	**64.7**	**3.0**	45	70.5	3.7

a: apatite; z: zircon Amount of helium is given in nano-cubic-cm in standard temperature and pressure. Amount of radioactive elements are given in nanograms.
Ejection correct. (Ft): correction factor for alpha-ejection (according to Farley et al., 1996 and Hourigan et al., 2005).
Uncertainties of helium and the radioactive element contents are given as 1 sigma, in relative error %.
Uncertainty of the single grain age includes both the analytical uncertainty and the estimated uncertainty of the Ft.
Uncertainty of the sample average age is given as 1 standard error (s.e.).

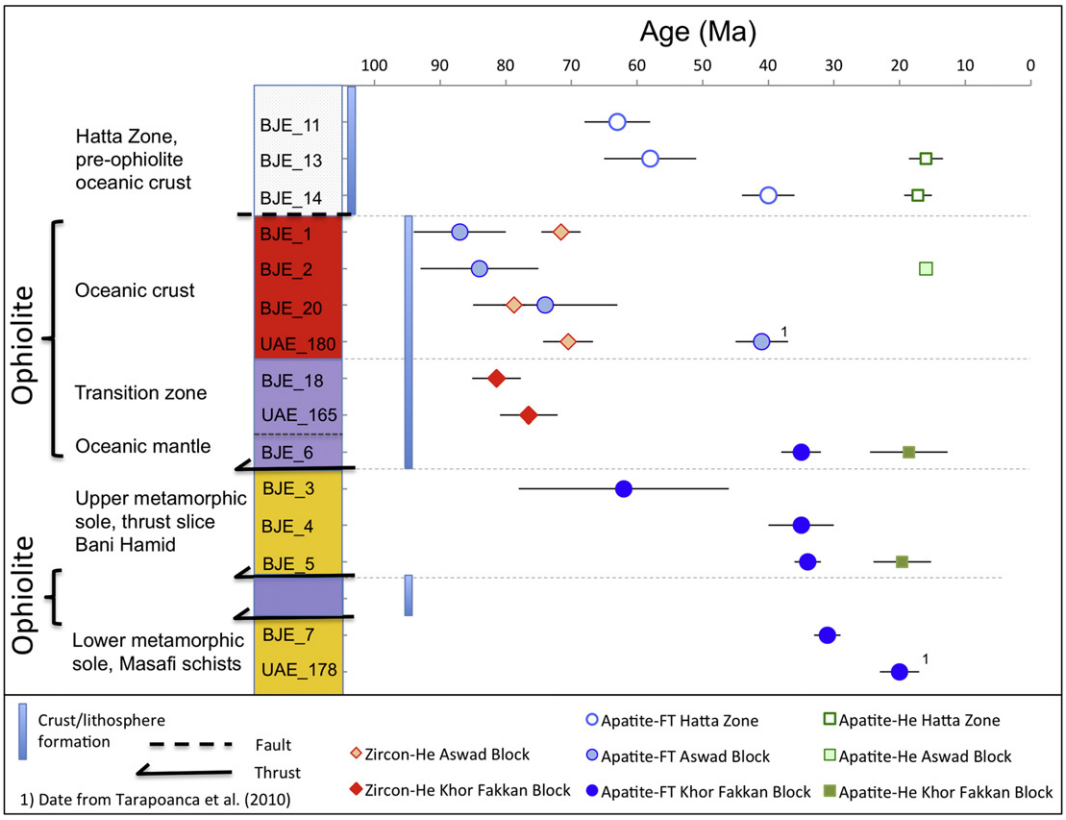

Fig. 6. Schematic representation of low-T thermochronological data with respect to relative structural level. Note, two dates are from Tarapoanca et al. (2010). Error bars are 1 σ. For colours in the geological column, refer to Fig. 4.

was generally poor. All analysed grains were very small, the geometries sometimes less than ideal (e.g. flat or rounded) and all grains included small inclusions. The older two ages are older than the AFT age from the same sample (35 Ma) and, regarding the analytical difficulties with this sample, we consider the group of the three younger ages to be more reliable. Similarly, five single grain ages from sample BJE_13 yielded an older (35–39 Ma) and a younger (14–19 Ma) age group. The ages show a negative correlation between age and grain size but no correlation between age and effective U-concentration. In the oldest grain a small inclusion was noted during grain selection, and a relatively high He re-extract indicates that this inclusion might have contributed to the total He of the analysis. The second oldest grain had a rather low U-concentration, so the three younger ages are considered more reliable; they provide a mean age of ca. 16 Ma. Finally, sample BJE_14 yielded four single grain ages between 14 and 19 Ma with a mean age of 17 Ma.

4.4. Modelled thermal histories

Three samples were chosen for thermal history modelling. Two samples come from the Khor Fakkan Block, from the metamorphic sole at Bani Hamid (BJE_05) and from a granite body in the lower part of the ophiolite (BJE_06). The third sample is a carbonatite from the Hatta Zone, Aswad Block (BJE_14). The selection criteria for the modelled samples included: a) availability of sufficient confined track length data through ^{252}Cf-irradiation (>50); b) precise fission-track age with sufficient number of single grain ages; and c) acceptable apatite (U–Th)/He age constraints, represented by little age scatter. For samples BJE_05 and 06, a first higher temperature constraint was placed at 75 ± 15 Ma and 140 ± 20 °C. This constraint is based on the consistent ZHe ages for five samples dated at ca. 75 Ma and an approximate effective closuring temperature for the ZHe system of ca. 150–140 °C for cooling rates of 1–2 °C/Ma (e.g. Reiners et al., 2004). For the end constraint a present day mean temperature range of 15–25 °C is assumed. For the carbonatite sample BJE_14, an initial low temperature constraint was placed close to the intrusion age of the carbonatite at ca. 103 Ma, taking into account that the carbonatite intruded into supracrustal rocks of the oceanic crust. A second, much wider constraint was placed to allow for burial/heating thereafter. This model also ends at present-day temperatures.

Sample BJE_05 from the metamorphic sole gave a reliable AFT age based on 25 single grain ages, along with three single grain apatite (U–Th)/He ages, with moderate scatter. The HeFTy model yielded 309 good-fit paths. The fit between the AFT data (age and track lengths) and the model is good; the fit for the AHe age is acceptable (Fig. 7c). Cooling into the AFT partial annealing zone (PAZ) is poorly constrained but occurred before ca. 40 Ma. The best-fit model suggests rapid cooling into the lower part of the AFT partial annealing zone (PAZ) at ca. 45 Ma, but many other good fit paths indicate that both earlier and later cooling is compatible with the data. A period of slow cooling followed until about 20 Ma, with cooling rates of ca. 1.1 °C/Ma. Another accelerated cooling step is recorded from ca. 20–15 Ma, followed by final exhumation to the surface, again at reduced exhumation rates.

Sample BJE_06 is from a granite that intruded into the lower part of the ophiolite above the Bani Hamid metamorphic sliver. The sample gave a precise AFT age based on 26 single grain ages. The AHe ages show significant scatter and only the group of three latest Oligocene–mid Miocene AHe ages was used for modelling. HeFTy modelling yields 430 acceptable paths, but no good paths. The time–temperature history is characterised by two rapid cooling steps at ca. 45–40 Ma and at ca. 20–15 Ma (Fig. 7b), with periods of slower cooling before 45 Ma, between 40 and 20 Ma and after 15 Ma. Since the modelling produced many acceptable paths, but no good paths, this might indicate that the t–T history maybe more complex than reflected by this simple model. The relatively poor quality of the apatites might be another reason for a slight misfit between AFT and AHe data.

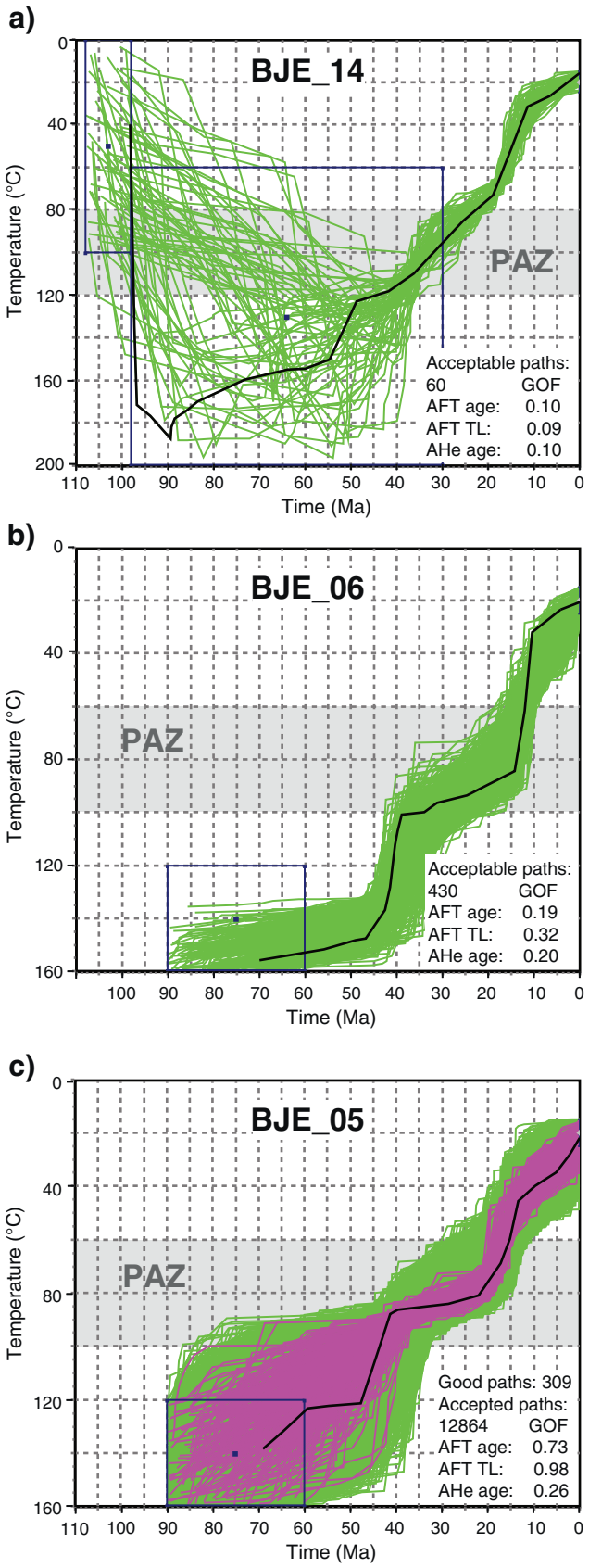

Carbonatite sample BJE_14, Hatta Zone, gave a reliable AFT age based on 24 single grain ages. It provided four consistent single grain (U–Th)/He apatite ages with little scatter. It was assumed that the Hatta volcanics were never overridden by the ophiolite (see first constraint in the modelling, Fig. 7a). Reheating to temperatures above the AFT PAZ sometime during the late Cretaceous–early Palaeogene erased all previous t–T history in the sample. Since cooling into the AFT PAZ at ca. 45 Ma, the sample experienced almost continuous moderate cooling to the surface. A slight acceleration of cooling is observed between 20 and 12 Ma. (Fig. 7a). Also for this sample, modelling yielded no good fit paths but a considerable number of acceptable fit paths (60).

5. Interpretations and discussion

The new thermochronological data are derived from two different ophiolite sections, the lower part including the metamorphic sole (Khor Fakkan Block) and the upper part of the ophiolite (Aswad Block); three samples characterise the non-ophiolitic uppermost oceanic crust in the faulted-bound Hatta Zone. ZHe data are restricted to the upper part of the ophiolite. From the three different thermochronological systems applied, the ZHe and AHe analyses revealed relatively consistent ages across the study area of ca. 80–70 Ma and 20–16 Ma, respectively (Fig. 6). The AFT data on the other hand have a wider scatter, ranging from 85–30 Ma across the Khor Fakkan and Aswad Blocks. The combined data probably reflect relatively simple cooling histories through the respective ZHe and AHe effective closing temperatures, whilst the AFT data record either more complex or slower cooling through the AFT–PAZ (120–80 °C).

5.1. Upper part of the ophiolite

The relatively uniform ZHe data of ca. 80–70 Ma, together with the three oldest AFT data of ca. 85–75 Ma from the higher part of the ophiolite are similar to Ar–Ar biotite data from similar levels (Hacker et al., 1996), indicating rapid cooling by 70 Ma to below ca. 140 °C and in part below 100 °C after the latest igneous activity, ophiolite obduction, and post-obduction folding. These data are consistent with the two oldest AFT ages of ca. 75 Ma reported by Tarapoanca et al. (2010). The combined ZHe and AFT data show that uplift, denudation and cooling to below 100 °C took place within about 10–20 Ma of ophiolite obduction, with post-obduction cooling rates of ca. 25–30 °C/Ma between 93 and 73 Ma. Tarapoanca et al. (2010) reported one zircon fission-track age of ca. 47 Ma from the same sample that was dated by ZHe in our study (UAE180). The zircon fission-track age of Tarapoanca et al. (2010) is apparently younger than the ZHe age, although the zircon fission track system has a higher closure temperature of ca. 280 °C. Since the zircon fission-track age is only based on 7 single grain analyses, we consider this age as potentially unreliable.

5.2. Base of the ophiolite

Metamorphic sole rocks at the base of the ophiolite underwent granulite facies metamorphism during short-lived continental margin subduction in the late Cretaceous, which attained temperatures up to 800–850 °C (Gnos and Kurz, 1994). During subsequent ophiolite obduction, peraluminous granites were generated at ca. 93 Ma, which

Fig. 7. Time–temperature models of three representative samples, from the structurally lowest level to the upper part of the ophiolite. The black line represents the best fit model. The purple paths represent paths with a good fit between model and data, the green paths have an acceptable fit. Modelling constraints are explained in chapter 4.4; a) BJE_14, carbonatite, Hatta volcanics, non-ophiolitic uppermost oceanic crust; b) BJE_06, granite, lower part of the ophiolite; c) BJE_05, metamorphic sole, quartzite, Bani Hamid. Abbreviations: AFT — apatite fission-track; TL — track length; AHe — apatite He; GOF — goodness of fit; PAZ — partial annealing zone.

required temperatures of at least 750 °C at the base of the ophiolite. As expected, the youngest AFT ages are from the structurally lowest section, the base of the ophiolite. AFT ages of ca. 35–30 Ma from this study indicate that the base of the ophiolite stayed at temperatures above 100 °C for a significant period of time after obduction. Thermal history models of two samples of the metamorphic sole (BJE_05) and from a granite within the lower part of the ophiolite (BJE_06) indicate that the metamorphic sole and the lower part of the ophiolite entered the apatite PAZ as late as the Eocene. The best-fit paths of both, BJE_05 and BJE_06, indicate rapid cooling into the lower part of the AFT–PAZ between ca. 45 and 40 Ma (Fig. 7b, c). The thermal history models indicate that the base of the ophiolite in the Khor Fakkan Block, was still at temperatures above 120 °C in earlier Eocene times, indicating at least 3–4 km of overburden at that time. A period of accelerated exhumation is recognised at ca. 45–40 Ma. Unfortunately, at present no ZHe data are available of the ophiolite base that would better constrain the T-history above the apatite PAZ. A single AFT age from the Masafi window gave a young age of ca. 20 Ma (Tarapoanca et al., 2010, Fig. 6), indicating that the deeper part of the metamorphic sole might have entered the AFT–PAZ as late as Miocene times.

5.3. Volcano-sedimentary rocks of the Hatta Zone

The volcano-sedimentary rocks of the Hatta Zone are equated with those of the Dibba Zone and represent the slope and deep-water Cretaceous Neotethyan rocks adjacent to the Arabian margin. They represent an in-faulted crustal block, separating the Aswad and Fizh ophiolite blocks. A volcanic/hypabyssal carbonatite was dated at 103 ± 1 Ma in the Masafi area (Grantham et al., 2003). Carbonatite dykes, assumed to be of the same age, intrude the sedimentary rocks of the Hatta Zone (Nasir and Klemd, 1998). As such, they should have cooled to surface temperature shortly after intrusion. However, AFT ages between ca. 60 and 40 Ma indicate that the dated samples either stayed at temperatures above 120 °C after emplacement or that the carbonatites underwent significant thermal overprinting after initial cooling to surface temperatures. A thermal history model of BJE_14 (Fig. 7a) indicates that the carbonatite sample entered the apatite PAZ for the last time at ca. 40 Ma, where it remained until it was exhumed to the surface in Neogene times.

5.4. Miocene AHe data

Five very similar AHe ages of ca. 16–20 Ma from the base of the ophiolite and from the Hatta Zone indicate a common Miocene exhumation event. The lower part of the metamorphic sole might have stayed at temperatures up to 100 °C until 20 Ma, as suggested by an AFT age of ca. 20 Ma from the Masafi schists (Tarapoanca et al., 2010).

5.5. Regional significance of thermochronological data

Ophiolite obduction initiated at ca. 93 Ma and tectonic exhumation was probably completed by 83 Ma. After another 10 Ma, by 73 Ma, large parts of the upper part of the ophiolite had quickly cooled to temperatures below ca. 100 °C, equivalent to cooling rates of 25–30 °C/Ma. Initially, ophiolite obduction might have been associated with significant topography, but subsequent loading caused downwarping of the Arabian lithosphere, leading to the formation of the westward propagating Aruma foreland basin. The lack of significant volumes of clastic detritus within the Aruma foreland basin probably indicates that ophiolite obduction was not immediately followed by large amounts of erosional unroofing. This observation is supported by the fact that the lower part of the ophiolite stayed at temperatures above 100 °C for some 40–50 Ma after obduction, indicating 3–4 km of long-lived overburden with respect to present outcrop levels. The period from ca. 70–45 Ma appears as a time of relative tectonic quiescence, although faults generated submarine relief and thus detritus with large ophiolite blocks was deposited along the eastern side of the Aruma basin (Ellison, 2014).

Numerous Eocene AFT ages from the base of the ophiolite and the metamorphic sole, as well as thermal history modelling indicates accelerated exhumation between ca. 45 and 35 Ma. This is coeval with early Zagros tectonism. At this time, the leading (southern) edge of Eurasia was beginning to thrust over the northern margin of Arabia. The shrinking remnants of Neotethys were represented by a marine accretionary prism, which was undergoing shortening and thrusting in approximately the position of the present Arabian Gulf (Mouthereau et al., 2012). A number of structures, originally related to obduction were reactivated during this time. Along the Wadi Ham Shear Zone, the Khor Fakkan Block was differentially exhumed with respect to the Aswad Block, which eventually led to exhumation of the metamorphic sole. The Palaeocene to Eocene AFT cooling ages of carbonatites of the Hatta Zone indicate that this area probably underwent reactivation and probably exhumation at this time. At the same time, the Ras Al Khaimah Basin was filled with up to 2000 m of Palaeocene to late Eocene sediments (Hasa and Pabdeh groups) and likely accommodated the erosional detritus documented by the exhumation revealed by the thermochronological data. Syn-sedimentary faults and thrust within the Ras Al Khaimah Basin indicate significant associated tectonism.

A Neogene exhumation step documented by four AHe ages finally exhumed the presently exposed outcrop levels close to the surface. This event is time equivalent with the main phase of the Zagros event. Since Neogene AHe ages are uniformly recorded from all five dated samples from the base of the ophiolite as well as from the Hatta Zone, this uplift event is likely associated with significant tectonism. The main phase of the Zagros orogeny is associated with a foreland fold and thrust belt that is responsible for this final exhumation event of the Oman Ophiolite. The erosional response of this exhumation event is probably reflected by the deposition of the Barzaman Formation, the lateral equivalents of which (Dam and Baynunah Formations) have been dated between 16 and 6 Ma respectively, by U–Pb carbonate dating (Farrant et al., 2012). The Barzaman Formation conglomerates are dominated by clasts derived from the ophiolite, but no metamorphic rock clasts are reported. This implies that the metamorphic rocks were probably still buried at this time.

6. Conclusions

The exhumation history of the Oman Ophiolite complex to present exposure levels in the Khor Fakkan and Aswad Blocks is the result of at least three distinct exhumation events:

1) The initial obduction from ca. 93–83 Ma is characterised by tectonic exhumation and rapid cooling; however it is not associated with major erosional exhumation. This is documented on the one hand by the developing sediment-starved Aruma Basin and on the other hand by the new thermochronological data that suggest that the ophiolite remained thick for a protracted time until at least ca. 45 Ma. A reason for this could be that ophiolite obduction might have never resulted in pronounced topography and therefore escaped significant erosion.
2) Thermochronological data from the lower part of the ophiolite and the metamorphic sole document a second exhumation event at ca. 45–40 Ma. This is time equivalent with the earlier stages of the Zagros orogeny that led to the reactivation of pre-existing structures. This event led to differential exhumation of the Khor Fakkan Block along the Wadi Ham Shear Zone. Unlike the initial obduction, this Zagros event resulted in significant erosional exhumation, during which 2000 m of sediments filled the Ras Al Khaimah Basin between Palaeocene and late Eocene times.
3) Finally, a Neogene exhumation step is recorded by ca. 20–15 Ma AHe data, the modelling, as well as a single AFT date from the lowermost metamorphic sole. This event can be linked to the main phase of the

Zagros orogeny, which saw large fans with ophiolite-derived debris (the Barzaman Formation conglomerates) issuing westwards from the Hajar Mountains. It also documents that the metamorphic sole of the Masafi window was still at temperatures in access of ca. 120 °C, corresponding to ca. 4 km of overburden. The main Zagros imprint was associated with reactivation of older structures and resulted in significant erosional unroofing. The present rugged topography seen in the Hajar Mountains is at least in part the result of a strong Neogene exhumation event related to the peak of the Zagros orogeny.

Acknowledgements

RJT thanks the UAE Ministry of Minerals and Energy (Saleh Al Mahmoodi, Khalid Al Hosani and Abdullah Gahnoog) who supported this study and the Director of BGS–NERC for permission to publish this article. JJ is grateful for BGS funding which enabled the sampling and analyses to take place. B. Kohn is thanked for the help with Cf-irradiation. M.-L. Balestrieri, F. Rouré and an anonymous reviewer are thanked for helpful reviews. Figs. 1, 3, 4 and 5 are from the © Ministry of Energy, UAE. Modified by BGS, © NERC2014.

References

Allen, P.A., 2007. The Huqf Supergroup of Oman: basin development and context for Neoproterozoic glaciation. Earth-Sci. Rev. 84, 139–185.
Bowring, S.A., Grotzinger, J.P., Condon, D.J., Ramezani, J., Newall, M.J., Allen, P.A., 2007. Geochronological constraints on the chronostratigraphic framework of the Neoproterozoic Huqf Supergroup, Sultanate of Oman. Am. J. Sci. 307, 1097–1145.
Cox, J., Searle, M.P., Pedersen, R., 1999. The petrogenesis of leucogranitic dykes intruding the northern Semail Ophiolite, United Arab Emirates: field relationships, geochemistry and Sr/Nd isotope systematics. Contrib. Mineral. Petrol. 137, 267–288.
Donelick, R.A., O'Sullivan, P.B., Ketcham, R.A., 2005. Apatite fission-track analysis. Rev. Mineral. Geochem. 58, 49–94.
Dumitru, T.A., 1993. A new computer-automated microscope stage system for fission-track analysis. Nucl. Tracks Radiat. Meas. 21, 557–580.
Dunkl, I., 2002. TRACKKEY: a Windows program for calculating and graphical presentation of fission track data. Comput. Geosci. 28, 3–12.
Ellison, R.A., 2014. New foreland basins are born. In: Thomas, R.J., Ellison, R.A. (Eds.), Geological Evolution of the United Arab Emirates. Over Six Hundred Million Years of Earth History. British Geological Survey, Keyworth, Nottingham, pp. 177–188.
Farley, K.A., 2000. Helium diffusion from apatite: general behavior as illustrated by Durango fluorapatite. J. Geophys. Res. 105 (B2), 2903–2914.
Farley, K.A., Wolf, R.A., Silver, L.T., 1996. The effects of long alpha-stopping distances on (U–Th)/He ages. Geochim. Cosmochim. Acta 60, 4223–4229.
Farrant, A.R., Ellison, R.A., Thomas, R.J., Pharaoh, T.C., Newell, A.J., Goodenough, K.M., Lee, J.R., Knox, R., 2012. The geology and geophysics of the United Arab Emirates. Geology of the Western and Central United Arab Emirates vol. 6. British Geological Survey (336 pp., The Geology and Geophysics of the United Arab Emirates, Memoirs, 6).
Gleadow, A.J.W., 1981. Fission-track dating methods: what are the real alternatives? Nuclear Tracks 5, 3–14.
Gnos, E., 1998. Peak metamorphic conditions in garnet amphibolites beneath the Semail Ophiolite: implications for an inverted pressure gradient. Int. Geol. Rev. 40, 281–304.
Gnos, E., Kurz, D., 1994. Sapphirine–quartz and sapphirine–corundum assemblages in metamorphic rocks associated with the Semail Ophiolite (United Arab Emirates). Contrib. Mineral. Petrol. 116, 398–410.
Goodenough, K.M., Styles, M.T., Schofield, D., Thomas, R.J., Crowley, Q.C., Lilly, R.M., McKervey, J.A., Stephenson, D., Carney, J.N., 2010. Architecture of the Oman–UAE ophiolite: evidence for a multi-phase magmatic history. Arab. J. Geosci. 3, 439–458.
Goodenough, K.M., Thomas, R.J., Styles, M.T., Schofield, D.I., MacLeod, C., 2014. Records of ocean growth and destruction in the Oman–UAE ophiolite. Elements 10, 105–110.
Grantham, G.H., Goedhart, M.L., Wipplinger, P.E., Thomas, R.J., Eglington, B.M., Harmer R.E., Hartzer F.J., 2003. The surface geology of the Emirate of Fujairah. Unpublished Report, Department of Industry and Economy, Government of Fujairah, United Arab Emirates, 455 pp.
Gray, D.R., Kohn, B.P., Gregory, R.T., Raza, A., 2006. Cenozoic exhumation history of Oman margin of Arabia based on low-T thermochronology. Goldschmidt Conference, Abs http://dx.doi.org/10.1016/j.gca.2006.06.428.
Hacker, B.R., Mosenfelder, J.J., Gnos, E., 1996. Rapid emplacement of the Oman Ophiolite: thermal and geochronological constraints. Tectonics 15, 1230–1247.
Hourigan, J.K., Reiners, P.W., Brandon, M.T., 2005. U/Th zonation dependent alpha ejection in (U–Th)/He chronometry. Geochim. Cosmochim. Acta 96, 3349–3365.
Hurford, A.J., Green, P.F., 1983. The zeta age calibration of fission-track dating. Chem. Geol. 41, 285–317.
Ketcham, R.A., 2005. Forward and inverse modelling of low-temperature thermochronometry data. Rev. Mineral. Geochem. 58, 275–314.
Ketcham, R.A., Carter, A., Donelick, R.A., Barbarand, J., Hurford, A.J., 2007a. Improved measurement of fission-track annealing in apatite using c-axis projection. Am. Mineral. 92, 789–798.
Ketcham, R.A., Carter, A., Donelick, R.A., Barbarand, J., Hurford, A.J., 2007b. Improved modeling of fission-track annealing in apatite. Am. Mineral. 92, 799–810.
Lal, D., Rajan, R.S., Tamhane, A.S., 1969. Chemical composition of nuclei Z > 22 in cosmic rays using meteoritic minerals as detectors. Nature 221, 33–37.
Lippard, S.J., Shelton, A.W., Gass, I.G., 1986. The ophiolite of Northern Oman. Memoir No. 11, The Geological Society. Blackwell Scientific, Oxford.
Mouthereau, F., Lacombe, O., Vergés, J., 2012. Building the Zagros collisional orogen: timing, strain distribution and the dynamics of Arabia/Eurasia plate convergence. Tectonophysics 532–535, 27–60.
Nasir, S., Klemd, R., 1998. New carbonatite occurrences along the Hatta transform fault zone (Northern Oman Mountains, United Arab Emirates). J. Afr. Earth Sci. 27, 3–10.
Nicolas, A., Boudier, F., Ildefonse, B., Ball, E., 2000. Accretion of Oman and United Arab Emirates ophiolite—discussion of a new structural map. Mar. Geophys. Res. 21, 147–179.
Peters, T., Kamber, B.S., 1994. Peraluminous, potassium-rich granitoids in the Semail Ophiolite. Contrib. Mineral. Petrol. 118, 229–238.
Rabu, D., 1993. Stratigraphy and Structure of the Oman Mountains. Doc. B.R.G.M. 221 p. 262.
Reiners, P.W., Spell, T.L., Nicolescu, St, Zanetti, K.A., 2004. Zircon (U–Th)/He thermochronometry: He diffusion and comparisons with 40Ar/39Ar dating. Geochim. Cosmochim. Acta 68, 1857–1887.
Rioux, M., Bowring, S., Kelemen, P., Gordon, S., Dudas, F., Miller, R., 2012. Rapid crustal accretion and magma assimilation in the Oman–UAE ophiolite: high precision U–Pb zircon geochronology of the gabbroic crust. J. Geophys. Res. 117. http://dx.doi.org/10.1029/2012JB009273.
Robertson, A.H.F., Blome, C.D., Cooper, D.W.J., Kemp, A.E.S., Searle, M.P., 1990. Evolution of the Arabian continental margin in the Dibba Zone, Northern Oman Mountains. In: Robertson, A.H.F., Scarle, M.P., Ries, A.C. (Eds.), The Geology and Tectonics of Oman Region. Geol. Soc. London, Spec. Publ. 49, pp. 251–284.
Searle, M.P., Cox, J., 1999. Tectonic setting, origin and obduction of the Oman Ophiolite. Geol. Soc. Am. Bull. 111, 104–122.
Searle, M.P., Malpas, J., 1982. Petrochemistry and origin of sub-ophiolite metamorphic and related rocks in the Oman Mountains. J. Geol. Soc. Lond. 139, 235–248.
Searle, M.P., Cherry, A.G., Ali, M.Y., Cooper, D.J.W., 2014. Tectonics of the Musandam Peninsula and northern Oman Mountains: from ophiolite obduction to continental collision. GeoArabia 19, 135–174.
Stern, R.J., Johnson, P., 2010. Continental lithosphere of the Arabian Plate: a geologic, petrologic, and geophysical synthesis. Earth Sci. Rev. 101, 29–67.
Styles, M.T., Ellison, R.A., Arkley, S.L.B., Crowley, Q., Farrant, A., Goodenough, K.M., McKervey, J.A., Pharaoh, T.C., Phillips, E.R., Schofield, D.I., Thomas, R.J., 2006. The geology and geophysics of the United Arab Emirates. Vol. 1: Geology. British Geological Survey, Keyworth, Nottingham (351 pp.).
Tarapoanca, M., Andriessen, P., Broto, K., Chérel, L., Ellouz-Zimmermann, N., Faure, J.-L., Jardin, A., Naville, C., Roure, F., 2010. Forward kinematic modelling of a regional transect in the Northern Emirates using geological and apatite fission track age constraints on Paleo-burial history. Arab. J. Geosci. 3, 395–411.
Thomas, R.J., Ellison, R.A., 2014. Geological evolution of the United Arab Emirates. Over Six Hundred Million Years of Earth History. British Geological Survey, Keyworth, Nottingham (287 pp.).
Thomas, R.J., Ellison, R.A., Goodenough, K.M., Roberts, N.M.W., Allen, P.A., 2015. Salt domes of the UAE and Oman: probing eastern. Precambrian Res. 256, 1–16.
Tilton, G.R., Hopson, C.A., Wright, G.E., 1981. Uranium–lead isotopic ages of the Semail Ophiolite, Oman, with applications to Tethyan ridge tectonics. J. Geophys. Res. 86, 2763–2775.
Warren, C.J., Parrish, R.R., Waters, D.J., Searle, M.P., 2005. Dating the geologic history of Oman's Semail ophiolite: insights from U–Pb geochronology. Contrib. Mineral. Petrol. 150, 403–422.